Nanoscale

Accepted Manuscript

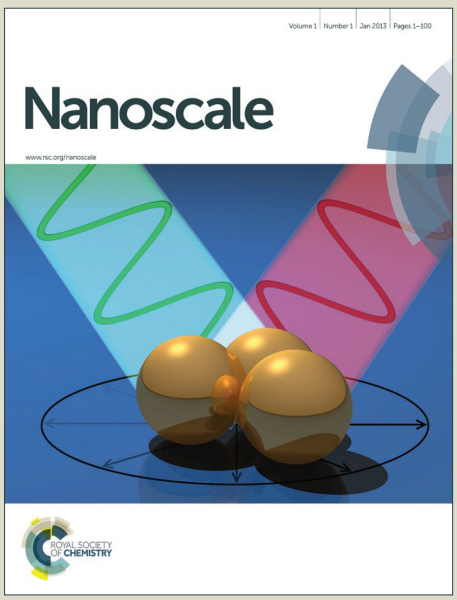

ROYAL SOCIETY OF CHEMISTRY

www.rsc.org/nanoscale

Nanoscale

Paper

Synthesis and Catalytic Properties of Highly Branched Palladium Nanostructures using Seeded Growth

Received 00th January 20xx,
Accepted 00th January 20xx

DOI: 10.1039/x0xx00000x

www.rsc.org/

L. Graham,[a] G. Collins,[b] J. D. Holmes,[b] and R. D. Tilley [a,c]

In order to develop nanocatalysts with enhanced catalytic performance, it is important to be able to synthesize nanocrystals enclosed by high-index surface facets, due to their high denisty of low coordinated atoms at step, ledge and kink sites. Here, we report a facile seed-mediated route to the synthesis of highly branched Pd nanostructures with a combination of {113}, {115} and {220} high-index surface planes. The size of these nanostructures is readily controlled by a simple manipulation of the seed concentration. The selective use of oleylamine and oleic acid was also found to be critical to the synthesis of these structures, with Pd icosahedra enclosed by low-index {111} facets being produced when hexadecylamine was employed as capping ligand. The structure-property relationship of these nanostructures as catalysts in Suzuki-cross coupling reactions was then investigated and compared, with the high-index faceted branched Pd nanostructures found to be the most effective catalysts.

Introduction

In industry, palladium is used extensively as a heterogeneous catalyst, especially for the reduction of automobile emissions,[1] and for carbon-carbon cross-coupling reactions such as Suzuki,[2-5] Heck,[6, 7] and Stille coupling.[8, 9] Suzuki cross-coupling reactions are one of the most widely implemented methods used in the formation of carbon-carbon bonds, and are also very efficient under heterogeneous catalysis conditions.[10, 11]

It is well established that the nanocrystal morphology, which is related to the type of exposed crystal plane and atomic arrangement on the surface of the nanocrystal, influences the catalytic activity and selectivity.[12-15] The shape sensitivity of nanocatalysts is attributed to electronic and geometrical effects that influence adsorption energies and reaction pathways.[16] The chemisorption of reaction species can occur preferentially on step, ledge and kink sites due to their low coordination numbers and allow more energetically favourable transition states compared to close-packed surfaces.[17-20] In general, high index planes have a greater density of low coordinated atoms.[21-23] Therefore, in-order to develop catalytic materials with enhanced catalytic performance, it is important to be able to synthesize nanocrystals enclosed by high-index planes rather than ones enclosed by more stable, low index-planes such as {111} and {100}.

High-index planes can be observed on highly branched nanocrystals such as multipod and dendritic structures.[24-26] The challenge, however, is there is no intrinsic driving force for catalytic metals that crystallize in a face-centered cubic (fcc) structure, to form these highly anisotropic structures. As a result, the formation of highly branched nanostructures requires growth under conditions that typically favour kinetic products.

To date, a range of branched nanostructures have been synthesized for various noble metals, including Pt,[27-29] Pd,[3, 30-32] Au,[33, 34] Ag,[35] and Ru.[36] However, the fast rate of kinetically controlled growth makes it difficult to control the final particle size, with branched structures >100 nm being produced. As a result, this decreases the relative surface area of the nanostructures, which is undesirable for catalytic applications.[2, 35, 37]

Here, we outline a simple seed-mediated route to the synthesis of highly branched Pd nanostructures enclosed by high-index surface planes. It was found that the size of the branched Pd nanostructures can be controlled by a simple manipulation of the seed concentration, rather than having to find means to manipulate the growth kinetics. We have also demonstrated how the overgrowth process, and hence final morphology of the Pd nanostructures is dictated by the selection of organic capping ligands present in the reaction

[a] School of Chemical and Physical Sciences, and The MacDiarmid Institute for Advanced Materials and Nanotechnology, Victoria University of Wellington, Kelburn Pde, Wellington 6012, New Zealand.
[b] Department of Chemistry and The Tyndall National Institute, University College Cork, Cork, Ireland.
[c] School of Chemistry and Mark Wainwright Analytical Centre, University of New South Wales, Sydney 2031, Australia. Tel: +61 (2) 9385 4435, Email: r.tilley@unsw.edu.au.

† Electronic Supplementary Information (ESI) available: TEM images of Pd seeds and nanocrystals synthesized using only oleylamine & oleic acid, catalytic reaction profiles, and details of TON & TOF calculations. See DOI: 10.1039/x0xx00000x

media, where it was found that changing the local ligand environment resulted in highly faceted Pd icosahedra. The structure-property relationship of these nanostructures as catalysts for the important Suzuki cross-coupling of phenylboronic acid and 4-methoxyiodobenzene/4-methoxybromobenzene was then investigated. The catalytic reactivity of Pd icosahedra with low-index {111} facets and branched nanostructures with a combination of high-index {113}, {115} and {220} facets were compared, with the high-index faceted branched Pd nanostructures found to be the most effective.

Experimental

Synthesis of Pd seeds

5.8 ± 0.4 nm Polycrystalline Pd seeds were synthesized from a heating-up method (Supporting Information Figure S1).[38] Typically, $Pd(acac)_2$ (0.33 mmol; Aldrich 99%) dissolved in trioctylphosphine (0.5 mL; Aldrich, 97%) was decomposed in the presence of oleylamine (5 mL, Aldrich, 70%) at 270°C for 30 minutes under a nitrogen atmosphere. The seeds were washed five times with equal amounts of methanol and toluene by centrifugation at 14,000 RPM (or 18,407 g) for 10 mins.

Synthesis of highly branched Pd nanocrystals

Bis(acetonitrile)dichloropalladium(II) ($PdCl_2(CH_3CN)_2$); 0.1 mmol; Aldrich, 99%) was dissolved in toluene in the presence of oleylamine (0.5 mmol, ACROS Organics 80 – 90%) and oleic acid (0.5 mmol, Aldrich 90%) in an 11 mL sample vial. The Pd seeds, suspended in toluene (0.00125 mmol) were then added, with a total solvent volume of 1 mL. The vial was then placed in a 10 oz. pressure reaction vessel filled with 10 mL excess toluene and sealed with bivalves. Air was evacuated from the bottle and then repeatedly purged with hydrogen gas (1 bar). The bottle was then filled with hydrogen gas (3 bar) and placed in a laboratory oven at 25°C for 2 hours. The gas was then released, and the solution was washed twice, with equal amounts of methanol and toluene, by centrifugation at 14,000 RPM (or 18,407 g) for 10 mins.

Synthesis of Pd icosahedra nanocrystals

The Pd icosahedra nanocrystals were synthesized according to the protocol for the highly branched Pd nanocrystals, however, the oleylamine/oleic acid was replaced with 10 eq. hexadecylamine (1 mmol, Aldrich 90%).

Pd nanocrystal characterization

Low-resolution TEM images were recorded using a JEOL 2010 electron microscope operated at 200 kV. High-resolution TEM images were recorded using a JEOL 2100F Field Emission Microscope. The TEM samples were prepared by re-dispersing the samples in toluene, then drop-wise addition of the liquid sample onto 400 mesh carbon-coated copper TEM grids. In some cases, the branched nanostructures were dispersed in dichloromethane (DCM). The fast evaporation of DCM prevented particle aggregation on the TEM grids, however, it also resulted in an oily residue on the surface of the grids. X-ray diffraction (XRD) data was obtained using a PANalaytical Xpert Pro MPD diffractometer system equipped with Cu-Kα radiation (Panalytical B.V., The Netherlands).

Catalyst preparation and surface cleaning

Two methods were employed for surfactant removal and surface cleaning. (1) Chemical washing: The as-synthesized Pd NC's were washed with toluene via sonication and vigorous stirring at RT for 30 min, and then collected by adding methanol and centrifugation at 14000 RPM (or 18,407 g). This procedure was repeated 3 times, before drop wise addition to a vigorously stirring solution of Darco D-60 activated carbon (Aldrich). This was then left stirring overnight at room temperature, then collected by filtration. (2) Thermal annealing: The Pd catalysts were added to the carbon black "un-washed" following the above procedure. The NC loaded onto the carbon support were then heated in a tube furnace for 3 h at 200°C.[39] The metal loading was calculated to give a 2 wt% metal/carbon catalyst loading.

Catalytic testing

In a typical reaction phenylboronic acid (1.1 mmol; 0.134 g), 4-methoxyiodobenzene (1 mmol; 0.234 g) or 4-methoxybromobenzene (1 mmol; 0.125 mL), and K2CO3 (2 mmol; 0.276 g) were added to 30 mL of ethanol/water (3:1). The reactions were initiated by addition of the catalyst. Reactions were conducted at room temperature (25°C) and 50°C and sampled at regular intervals for GC analysis. Samples were analyzed using an Agilent 7890A GC system, equipped with a flame ionization detector (FID). Products were identified against authenticated standards and quantified by calibration to obtain response factors (RF) against the known internal standard (dodecane). The turnover number (TON) and turnover frequency (TOF) were calculated on the basis of amount of biaryl product formed and normalized to the number of surface Pd atoms. Please refer to the Supporting Information for more details.

Results and Discussion

The underlying principles to synthesizing branched nanostructures requires growth under kinetic control – where the rate of adatom addition far exceeds that of adatom diffusion, resulting in high-energy facets growing more quickly than low-energy facets. Previous work from our group by Watt *et al* found that varying the nature of the organic capping system enabled the control of the growth kinetics and resulted in the formation of highly branched Pd nanostructures that were larger than 85 nm, through a homogeneous nucleation route.[40] Here, we have adapted the methodology employed by Watt *et al*, with the intention of synthesizing branched Pd nanostructures of smaller more controlled sizes, and with less extensive branching in order to form materials with a high surface-area and high-index surface facets that are readily

available for catalytic reactions. We approached this challenge by introducing a pre-formed Pd seed into the reaction, in order to obtain more control over the growth rates, and hence size and morphology of these highly branched nanostructures.

Initially, polycrystalline Pd seeds were synthesized via a heating-up method.[38] First, a Pd-Top complex was formed by reacting $Pd(acac)_2$ and TOP under N_2. This metal complex was then added to oleylamine, which acted as the reductant, capping ligand and solvent, and slowly heated to 270°C under N_2. The reaction solution was then aged for 30 min. A methanol/toluene mixture was used to precipitate the particles out of solution. Analysis by transmission electron microscopy (TEM) reveals that the seeds are polycrystalline and highly uniform, with an average diameter of 5.8 ± 0.4 nm (Figure S1 of the Supporting Information).

To grow the branched Pd nanostructures, the palladium seeds (0.00125 mmol) were added to a solution containing Bis(acetonitrile) palladium(II) dichloride, 1:1 oleylamine (OAm) and oleic acid (OA), and toluene. The reaction solution was then reduced under a hydrogen atmosphere (3 bar) in a 12 oz. pressure reaction vessel at room temperature for 2 hrs.

A representative low-resolution TEM image of the branched structures can be seen in Figure 1a. From the higher magnification TEM image of an individual branched nanocrystal (Figure 1b) it can be seen that the branches are well defined and spatially separated from each other. They extend radially from a central core, and the outer edge and tips of the branches are much brighter than the center region of the nanocrystal. This difference in contrast indicates that the edge and tips of the branches are much thinner than the central region of the nanocrystal. The average size of the branched nanocrystals was found to be 37 ± 9 nm, which is more controlled and smaller than those synthesized by Watt *et al* using a non-seeded route.[40] This was obtained from TEM analysis (Figure 1c), by measuring the distance from the longest apex - apex length for each of the branched nanocrystals. Figure 1d shows a HRTEM image of a single crystallite branch. From this, it can be seen that the branch contains continuous atomic lattices throughout the entire length of the branch indicating it is single crystalline.The presence of discreet spots displayed in the corresponding FFT (shown in inset) also confirms the branch is single crystal, and that the branch is viewed down a <110> zone axis, with branch growth in the <110> direction. The single crystal nature of the branches indicates that they are formed via adatom addition and direct growth on the Pd seed rather than by the random aggregation of smaller nuclei. Figure 1e shows a magnified image of the region inside the red rectangle in Figure 1d. Upon analysis of the atomic packing, it can be seen that the particles contain extensive high-index faceting. The facets on the branch surface were found to consist of a series of {111} and {002} facets, which combine to form the high index {113}, {115} and {220} facets, which is also shown schematically in the two-dimensional lattice model in Figure 1f. The XRD pattern for the carbon supported branched Pd nanostructures (Figure S2 of the Supporting Information) also supports these results, which shows diffraction peaks at 40.1°, 46.6°, 68.1° which are assigned to the (111), (200, (220) crystal facets for face centered cubic (fcc) Pd crystal structure.

To further elucidate the growth mechanism of these highly branched nanostructures, time-dependent reactions were

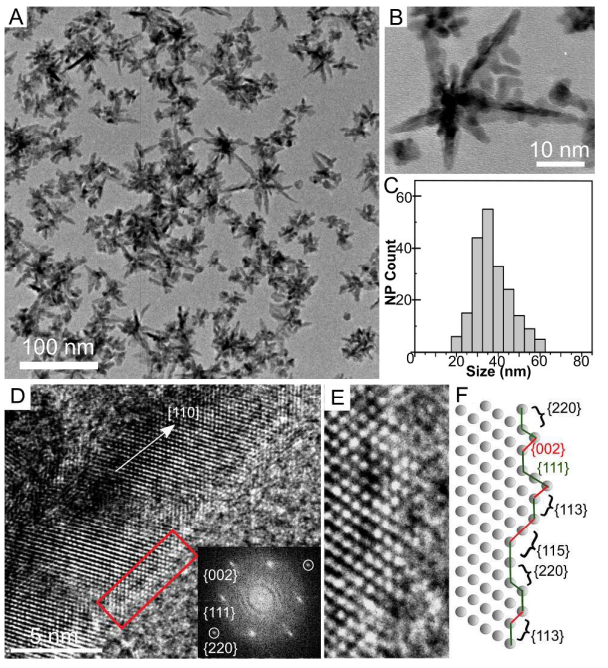

Figure 1. a) Low-resolution TEM image of the branched Pd nanocrystals; b) HRTEM image of a single branched nanostructure; c) Size distribution indicating the branched particles have an average size of 37± 9 nm; d) HRTEM image of a single branch, with the FFT in the inset showing it is being viewed down a {110} zone axis and that the branch is growing in the <110> direction; e) Magnified image of the region inside the red rectangle in 1d; f) Two-dimensional lattice model of the TEM image in e) illustrating the high-index {113}, {115} and {220} facets.

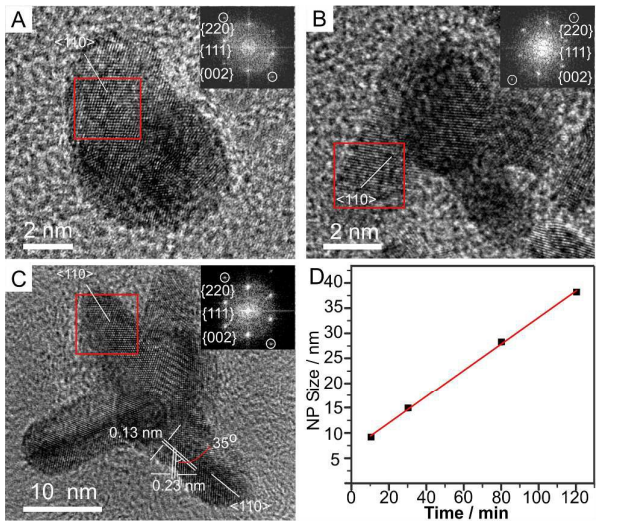

Figure 2. HRTEM images showing the time evolution of the highly branched nanostructures: a) Particle obtained at t = 10 min, showing early signs of branching in the <110> direction according to the FFT in the inset; b) Particle obtained after t = 30 min, with branch growth in the <110> direction according to the FFT in the inset; c) Particle obtained after t = 80 min, with branch growth in the <110> direction according to the FFT in the inset; d) Plot of the average size of reaction intermediates formed vs. reaction times, indicating a linear relationship.

carried out to isolate the intermediates formed during the reaction. Reaction times were shortened to 10, 30, and 80 min. TEM images of individual nanoparticles obtained from these reaction times can be seen in Figure 2a, b and c respectively. The fully formed branched nanocrystals obtained from a reaction time of 120 min are shown in Figure 1. Figure 2a shows a HRTEM image of a 9 nm nanocrystal obtained from a reaction time of 10 min. From this, the early growth of a single branch can be observed. The power spectrum shown in the inset corresponds to the area of the branch inside the red box, and shows that the nanostructure is viewed down a <110> zone axis. Figure 2b shows a HRTEM image of a 14.7 nm nanocrystal obtained from a reaction time of 30 min. From this, it can be seen that the formation of multiple branches start to appear. The FFT in the inset corresponds to the area inside the red box, and indicates that the branch is being viewed down a <110> zone axis, with the branch also growing in the <110> direction. Figure 2c shows a HRTEM image of a single nanocrystal obtained from a reaction time of 80 min. The nanocrystal is 28 nm in size, and consists of multiple branches extending radially from a central core. From the HRTEM image, the presence of a {110} twin plane can be seen running along the entire length of the two bottom branches. Upon analysis of the atomic packing on the bottom right branch, lattice spacings of 0.13 nm and 0.23 nm were measured, and indexed to the {220} and {111} reflections of face-centered cubic (fcc) Pd. The angle between these two atomic lattices was found to be 35° indicating that the branch is being viewed along a <110> zone axis, with the branch growing in a <110> direction. The power spectrum in the inset corresponds to the area of the top-right branch in the red box and indicates that the branch is also being viewed down a <110> zone axis, with branch growth occurring in the <110> direction. From the time resolved TEM images and Figure 2d, it can be seen that there is a linear relationship between the reaction time and size of the synthesized branched nanostructures. This indicates that there is a constant supply of Pd monomer to the growing surface of the NC over the 120 min period. From Figure 2, it can be seen that the branches start to appear at an early stage (10 min) and continue to grow into larger and more distinctive branches over time. This result also confirms that the branches are formed via adatom addition and direct growth on the Pd seed.

In order to obtain more control over the size of the Pd branched structures, a range of experiments using different seed concentrations were carried out to investigate the effect this has on the size and morphology of the resultant nanoparticles. Alternative seed concentrations of 0.005, 0.0025, and 0.0005 mmol were added to the reaction solution, with all other reaction conditions being kept constant. The results are shown in Figure 3. When a high seed concentration of 0.005 mmol was used (Figure 3a), the formation of small branches is evident. A HRTEM image of a single particle can be seen in Figure 3b. From this, it can be seen that the small branches are extending radially away from the central core. Again, a difference in contrast is observed between the core and the branch arms of the particle, indicating that the there is

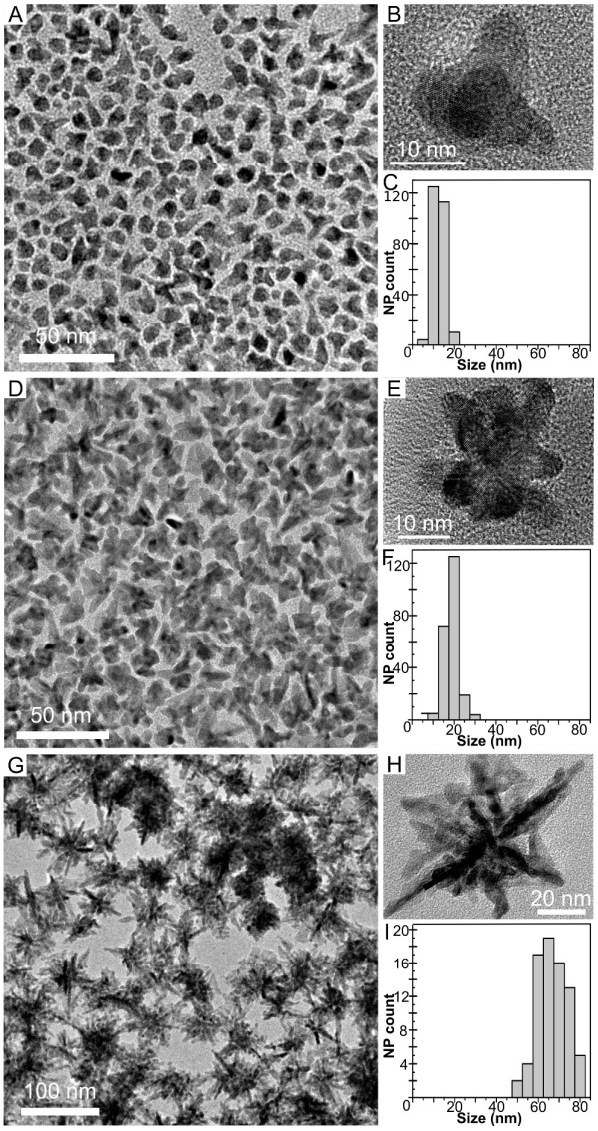

Figure 3. Branched Pd nanostructures produced from varying Pd seed concentrations: a) Low-resolution TEM image of branched Pd nanocrystals produced from a seed concentration of 0.005 mmol, particles have an average size of 12.5 nm as indicated from the histogram in c), b) HRTEM image of a single particle produced from 0.005 mmol seed concentration. d) LRTEM image of branched Pd nanocrystals produced from a seed concentration of 0.0025 mmol, particles have an average size of 25 ± 3 nm as indicated from the histogram in f), e) HRTEM image of a single particle produced from 0.0025 mmol seed concentration. g) LRTEM image of branched Pd nanocrystals produced from a seed concentration of 0.0005 mmol, particles have an average size of 69 ± 15 nm as indicated from the histogram in f).

more Pd at the centre of the particles than in the branches. The average size of these nanocrystals were found to be 12.5 nm, as shown by the size distribution in Figure 3c. With a seed concentration of 0.0025 mmol, the sample appears to be more uniform in size and morphology (Figure 3d) and the average size of the branched nanocrystals increases to 25 ± 3 nm (Figure 3f). When a really low seed concentration is employed, such as 0.0005 mmol, the branched nanocrystals have further increased in size to 69 ± 15 nm as seen in Figure 3g and the

corresponding size distribution in Figure 3I. It should also be noted; when the seed concentration was reduced even further (< 0.0005 mmol), homogeneous nucleation was no longer suppressed with the formation of small Pd nuclei appearing. From analysis of Figure 2 and 3, it appears that the polycrystalline seeds provide multiple nucleation sites for Pd monomers that are spatially separated from each other in order to avoid overlap and fusion, and allow the formation of these Pd branched nanostructures with an open dendritic structure. It also appears that the nanostructures undergo high growth rates at areas of high curvature, such as at the tips and edges of the branches. This is in accordance with a kinetic growth regime, where the rate of monomer addition to the nanocrystal surface far exceeds that of adatom diffusion around the growing nanocrystal surface.[41, 42] It may also be observed that the overall size of the branched nanocrystals can be readily controlled by changing the concentration of the pre-formed polycrystalline seeds present in the reaction solution.

It has been well established that two of the most important factors influencing the growth of highly anisotropic nanostructures are (1) the monomer concentration in solution,[41, 43, 44] and (2) the ability of shape directing agents such as organic capping ligands to bind to various nanocrystal facets with different affinities, influencing their relative stabilities.[26, 45] In these experiments, the critical role of the seed concentration in determining the size of the branched nanostructures is shown in Figure 3. A high seed concentration (0.005 mmol and 0.0025 mmol) present in the reaction solution results in an increase in the number of nucleation sites on the seeds for adatom addition, resulting in less monomer available for subsequent growth, and hence smaller branched structures. Conversely, when the seed concentration is reduced (0.0005 mmol), the number of nucleation sites on the seeds for monomer addition is also reduced, resulting in more monomer available for growth, and hence larger branched structures being produced. Peng and co-workers also noted similar results in the synthesis of CdSe nanorods, where they found that the aspect ratios and length of the CdSe nanorods could be tuned by changing the monomer concentration in solution.[44] Zhong and co-workers also observed similar results in the synthesis of anisotropic nanostructures synthesized from gold seeds.[41]

In addition to the monomer concentration in solution, we have also investigated the sensitivity of these anisotropic branched structures to the capping ligands employed. When only OA was used as the capping ligand, large (> 0.2 μm) branched Pd structures were produced (Figure S3 of the Supporting Information). In contrast, when the capping ligand was changed to only OAm, polyhedral and plate-like Pd structures were produced, which is consistent with previous finidings in the literature (Figure S3 of the Supporting Information).[40, 46, 47] This was expected, as the carboxylic acid functionality of OA possesses a weaker binding strength to palladium compared to the amine functionality of the OAm, allowing a greater flux of monomers to the surface of the growing nanocrystal. These results show that the selective use

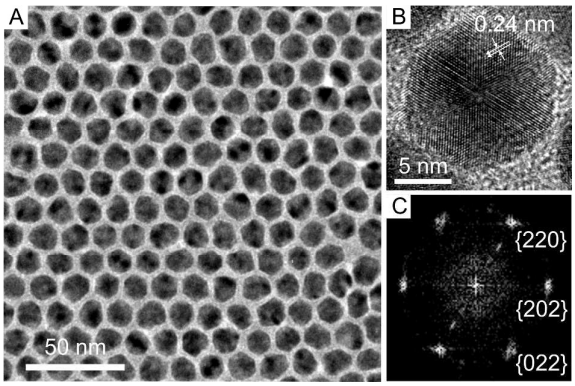

Figure 4. a) Low-resolution TEM image of the icosahedra formed using HDA as the capping ligand; b) HRTEM image of a single icosahedron, viewed along a <111> zone axis as indicated by the corresponding FFT shown in c).

of oleylamine and oleic acid is critical to the synthesis of these highly branched structures. This dual ligand system has also been found by other groups to be essential in the formation of desired nanocrystals.[48-52] When the capping ligand was changed to hexadecylamine (HDA; a straight chain amine) thermodynamically controlled icosahedra were formed as can be seen in Figure 4. Figure 4a shows a low magnification TEM image of the Pd icosahedra. From TEM analysis, they were found to be 12.9 ± 0.7 nm in size and monodisperse with well-defined faceting and display a hexagonal projection. Some irregularity in particle shape is observed, which we believe is due to the different growth rates on different facets of the intrinsically polycrystalline Pd seeds. Figure 4b shows a high-resolution TEM (HRTEM) of a single Pd icosahedron. The multiply twinned structure of an icosahedron is observed by the presence of twin planes on the surface of the nanocrystal which radiate out from a central axis. This indicates a threefold axis-oriented parallel to the electron beam. The lattice spacing of 0.24 nm on the surface of the icosahedron in 4b can be indexed to the {111} reflection of face-centered cubic (fcc) Pd. The spots of the corresponding fast Fourier transform (FFT) in Figure 4c show hexagonal symmetry and were indexed to {220} reflections, confirming that the nanocrystal in Figure 2b is indeed bound by {111} lattice planes. This change in morphology, from a highly branched nanostructure to one bound by {111} facets, is due to a combination of an increased binding strength and steric effects of the capping ligands. A special feature of OAm and OA is the cis double bond (C = C) in the middle of both the molecules. The steric hindrance of these ligands prevents them from packing as tightly around the growing nanocrystal surface as that of HDA. This, in turn, increases the collective binding strength, and also leaves less unpassivated areas on the growing nanocrystal surface on which monomers from the solution can add to. This results in a more diffusion controlled growth regime, where the rate of adatom diffusion on the surface of the growing nanocrystal exceeds the rate of atom deposition, thus resulting in thermodynamically produced icosahedra. Similar steric effects and electronic effects have previously been reported.[53] For example, Xia and coworkers found that substituting

octadecylamine (ODA) for OAm resulted in significantly different morphologies and crystallinities, even though ODA and OAm exhibit similar basicity and affinity to metals. Chaudret *et al* also observed less long-range organization with OAm compared to ODA.[54]

Of the diverse range of catalytic reactions that use Pd-based catalysts, the industrially important Suzuki-coupling reaction has been widely used as a model reaction to test the catalytic performance of Pd nanocrystals of various shapes,[55] sizes[10] and compositions.[56] Branched nanostructures with thin, long arms/branches are ideal for catalytic applications due to their often-large surface areas and multiple high-angle edges and sharp tips. Based on this, the Suzuki-coupling reaction was selected to test that complex morphologies, such as branched NC's with an abundance of high-index facets are more effective catalysts than structures enclosed by low-index facets (Pd icosahedra). This preliminary study is in-line to those carried out by other groups with similar samples.[32, 57, 58]

While the capping ligands employed during a NC synthesis are key to shape-control and preventing aggregation, they can also be detrimental to the catalytic activity by blocking access of reactant molecules to the active surface atoms. Therefore, it is of the highest importance to 'clean' the NC surfaces without inducing structural changes. Two methods were employed for capping ligand removal and surface cleaning of the nanocrystals. The Pd NC's were washed with toluene using sonication and vigorous stirring at RT for 30 min, and then collected by adding methanol as a non-solvent and centrifugation. This procedure was repeated 3 times. After that, the NC's were mixed with carbon black in toluene by sonication and stirring overnight. The solvent was then evaporated at room temperature in air. This powder was denoted as "untreated" catalyst. From the TEM images (Figure S4 of the supporting Information), There were no observed changes to the nanocrystal size and shape upon loading on the carbon support. The second treatment involved thermal annealing, and followed a protocol similar to that derived by Li *et al*.[39] The NC's were loaded onto the carbon black as above, "un-washed". The catalyst loaded on carbon was then heated in a tube furnace for 3 hours at 200°C in air. The TEM images of the NC's after heat treatment can be seen in Figure S5 of the Supporting Information. From this, it can be seen that the heat treatment induced structural changes with both the NC samples. Based on this, only the "untreated" samples were used for catalytic testing due to the NC's retaining their shape after washing and loading onto the carbon support.

Scheme 1. Model Suzuki-Miyaura reaction used in this study.

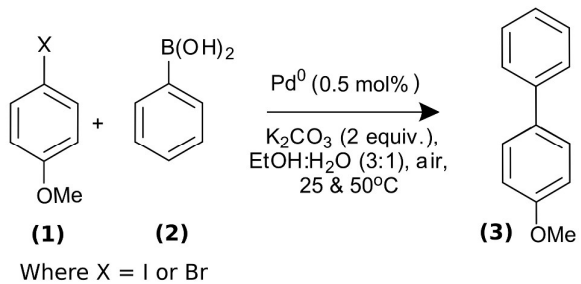

Table 1. Reaction yields, TON and TOF's per surface Pd atom of the Pd Icosahedra and branched Pd nanostructures in Suzuki Coupling.[a]

Catalyst	Reaction	Yield (%)	TON_{surf}	TOF_{surf} (min^{-1})
Pd Icosahedra NC	Ar-Br 25°C	37	564	3.1
	Ar-I 25°C	44	669	3.7
	Ar-Br 50°C	52	788	4.4
	Ar-I 50°C	90	1364	7.6
Branched Pd NC	Ar-Br 25°C	33	976	5.4
	Ar-I 25°C	50	1490	8.3
	Ar-Br 50°C	46	1360	7.6
	Ar-I 50°C	90	2661	14.8

[a] See Supporting Information for TON_{surf} and TOF_{surf} calculations.

The Suzuki coupling reaction was carried out at 25°C and 50°C, compared to 75°C - 85°C which is usually used for the coupling of either 4-methoxyiodobenzene (1) and 4-methoxybromobenzene with phenylboronic acid (2) to give 4-methoxybiphenyl (3), as seen in Scheme 1. In our experiment, the Pd nanocrystals were loaded onto the carbon support at 2 wt %, and the molar ratio of total Pd to 4-methoxyiodobenzene/4-methoxybromobenzene was just 0.5% compared to 1.7% used previously for Pd icosahedra (at 78°C and reaction time of 12hr) and 1.8% used previously for Pd branched structures (85°C and reaction time of 4 hrs).[59,2] The reaction yields after 3 h for the two types of Pd nanocrystals are listed in Table 1, and range from 33 – 90%. Very little biphenyl (yielding less than 1%) was detected in the absence of catalysts. When the catalytic reaction was carried out at 50°C, much higher yields (90%) of methoxybiphenyl (at least 1.4 x for 4- methoxybromobenzene and 1.8 x for 4-methoxyiodobenzene) were produced compared to those carried out at 25°C due to reaction kinetics being faster at elevated temperatures, for both the Pd icosahedra and the branched Pd nanostructures. To allow for the direct comparison of the effect of nanoparticle shape and surface structure on the catalytic activity, the surface normalized turnover numbers (TONs) and turnover frequencies (TOFs) for each Pd nanostructure were calculated,as shown in Table 1. N_2-adsoprtion measurements were performed to determine the surface area of the branched Pd samples, however owing to the aggregation and coalescence during the drying process, and the particles being loaded on a carbon support, the results were unreliable. Up to 200 individual metal particles were counted for each sample to determine the average nanocrystal diameter. The number of surface atoms on the branched Pd NS and Pd Icosahedra was calculated on the basis of geometrical considerations assuming a face-centered cubic (fcc) Pd lattice. This approach has been widely used to calculating surface area and the number of surface atoms present on NC of various morphologies.[2, 12, 56, 60, 61] The

calculation details are provided in the Supporting Information. As shown in Table 1, the branched nanostructures display enhanced catalytic performance in all the cross-coupling reactions evaluated. The TOFs for the icosahedra in the cross coupling of 4-methoxyiodobenzene at 50°C was 7.6 min^{-1}, which more than doubled to 14.8 min^{-1} for the branched nanostructures under the same conditions. A similar trend in increased TOFs was observed for the reaction carried out at 25°C. For the cross coupling of 4-methoxybromobenzene, slightly lower TOFs and longer lag times of at least 30 min (Figure S6 of the supporting -information) were obtained compared to their iodo- counterparts (lag time of 5 min). No difference in the induction period with the different capping ligands employed, with the one exception of the HDA capped Pd Icosahedra catalysing 4-methoxybromobenzene at 50°C. In this case, the induction period increases to 60 minutes, indicating there may be a change in the catalytic mechanism involved. The TOFs for the branched nanostructures at both 25 and 50°C for the cross coupling of 4-methoxyiodobenzene increase by at least 1.7x respectively compared to the TOFs obtained from the icosahedra. These results are expected, as aryl iodides will generally undergo faster oxidative addition than electron deficient aryl bromides. High-index surface facets exhibit a large number of steps, kinks and ledges which contain a high number of Pd atoms at these sites which are more co-ordinately unsaturated than those present on lower-index facets, which often results in increased catalytic activity. Therefore, we believe the higher catalytic activity of the branched Pd nanostructures is most likely ascribed to the higher reactive nature of the {113}, {115} and {220} high-index facets compared to that of the low-index {111} facets present on the Pd icosahedra. This large TOF difference between the branched nanostructures and icosahedra clearly demonstrates the importance of controlling the exposed facets and hence morphology of the nanocrystals for the optimization of catalytic performance.

Conclusions

In conclusion, this paper illustrates a simple seed-mediated method for the synthesis of highly branched Pd nanostructures with high-index surface planes. The size of the branched Pd nanostructures was controlled by the simple manipulation of the seed concentration, rather than manipulating the growth kinetics, which enabled far smaller and more monodispersed, 37 ± 9 nm, branched nanostructures to form. Additionally it has been shown that the overgrowth process, and final morphology of the Pd nanostructures is dictated by choice of organic capping ligands used in the reaction. As a result, structures ranging from highly branched Pd nanostructures to small highly faceted Pd icosahedra were produced. The structure-property relationship of these nanostructures as catalysts has been shown for the industrially important Suzuki cross-coupling of phenylboronic acid and 4-methoxyiodobenzene/4-methoxybromobenzene. The catalytic reactivity of Pd icosahedra with low-index {111} facets and branched nanostructures with a combination of high-index {113}, {115} and {220} facets were compared, with the high-index faceted branched Pd nanostructures found to be the most effective. These results provide strong evidence of the importance of high-index facets and uncoordinated surface atoms in carbon-carbon bond forming catalytic reactions and shed light on the underlying relationship between nanocrystal surface structures and their intrinsic catalytic activities. The seed-mediated and ligand-controlled approach described provides a powerful tool that can facilitate the size-controlled synthesis of highly branched Pd nanostructures. We believe the principles outlined here will hold for other monometallic and bi-metallic seed-mediated systems as well, enabling the controlled synthesis of a range of highly branched high-index faceted nanostructures that should be highly suited for enhanced catalytic performance.

Acknowledgements

L.G and R.D.T would like to thank the MacDiarmid Institute for funding.

References

1. Y. Nishihata, J. Mizuki, T. Akao, H. Tanaka, M. Uenishi, M. Kimura, T. Okamoto and N. Hamada, *Nature*, 2002, **418**, 164-167.
2. Y.-H. Chen, H.-H. Hung and M. H. Huang, *J. Am. Chem. Soc.*, 2009, **131**, 9114-9121.
3. F. Wang, C. Li, L.-D. Sun, C.-H. Xu, J. Wang, J. C. Yu and C.-H. Yan, *Angew. Chem., Int. Ed.*, 2012, **51**, 4872-4876.
4. J. P. Wolfe, R. A. Singer, B. H. Yang and S. L. Buchwald, *J. Am. Chem. Soc.*, 1999, **121**, 9950-9561.
5. M. Pérez-Lorenzo, *J. Phys. Chem. Lett.*, 2012, **3**, 167-174.
6. G. Zhang, H. Zhou, J. Hu, M. Liu and Y. Kuang, *Green Chem.*, 2009, **11**, 1428-1432.
7. A. Kamal, V. Srinivasulu, B. N. Seshadri, N. Markandeya, A. Alarifi and N. Shankaraiah, *Green Chem.*, 2012, **14**, 2513-2522.
8. D. B. Pacardo, M. Sethi, S. E. Jones, R. R. Naik and M. R. Knecht, *ACS Nano*, 2009, **3**, 1288-1296.
9. J. C. Garcia-Martinez, R. Lezutekong and R. M. Crooks, *J. Am. Chem. Soc.*, 2005, **127**, 5097-5103.
10. A. Fihri, M. Bouhrara, B. Nekouesishahraki, J.-M. Basset and V. Polshettiwar, *Chem. Soc. Rev.*, 2011, **40**, 5181-5203.
11. Y. Wu, D. Wang and Y. Li, *Chem. Soc. Rev.*, 2014, **43**, 2112-2124.
12. D. Shuai, D. C. McCalman, J. K. Choe, J. R. Shapley, W. F. Schneider and C. J. Werth, *ACS Catal.*, 2013, **3**, 453-463.
13. S. Cai, H. Duan, H. Rong, D. Wang, L. Li, W. He and Y. Li, *ACS Catal.*, 2013, **3**, 608-612.
14. K. M. Bratlie, H. Lee, K. Komvopoulos, P. Yang and G. A. Somorjai, *Nano Lett.*, 2007, **7**, 3097-3101.
15. S.-I. Choi, J. A. Herron, J. Scaranto, H. Huang, Y. Wang, X. Xia, T. Lv, J. Park, H.-C. Peng, M. Mavrikakis and Y. Xia, *ChemCatChem*, 2015, **7**, 2077-2085.

16. Z.-P. Liu and P. Hu, *J. Am. Chem. Soc.*, 2003, **125**, 1958-1967.
17. M. Crespo-Quesada, A. Yarulin, M. Jin, Y. Xia and L. Kiwi-Minsker, *J. Am. Chem. Soc.*, 2011, **133**, 12787-12794.
18. Y. Xiong, J. M. McLellan, Y. Yin and Y. Xia, *Angew. Chem., Int. Ed.*, 2007, **46**, 790-794.
19. L. M. Falicov and G. A. Somorjai, *Proc. Natl. Acad. Sci. U.S.A.*, 1985, **82**, 2207-2211.
20. T. A. Baker, B. Xu, S. C. Jensen, C. M. Friend and E. Kaxiras, *Catal. Sci. Technol.*, 2011, **1**, 1166-1174.
21. M. Jin, H. Zhang, Z. Xie and Y. Xia, *Angew. Chem., Int. Ed.*, 2011, **123**, 7996-8000.
22. Q. Zhang and H. Wang, *ACS Catal.*, 2014, **4**, 4027-4033.
23. Z. Quan, Y. Wang and J. Fang, *Acc. Chem. Res.*, 2012, **46**, 191-202.
24. J. Lai, W. Niu, W. Qi, J. Zhao, S. Li, W. Gao, R. Luque and G. Xu, *ChemCatChem*, 2015, **7**, 1064-1069.
25. B. Lim, M. Jiang, P. H. C. Camargo, E. C. Cho, J. Tao, X. Lu, Y. Zhu and Y. Xia, *Science*, 2009, **324**, 1302-1305.
26. C. J. DeSantis and S. E. Skrabalak, *J. Am. Chem. Soc.*, 2012, **135**, 10-13.
27. S. Cheong, J. Watt, B. Ingham, M. F. Toney and R. D. Tilley, *J. Am. Chem. Soc.*, 2009, **131**, 14590-14595.
28. L. Ma, C. Wang, M. Gong, L. Liao, R. Long, J. Wang, D. Wu, W. Zhong, M. J. Kim, Y. Chen, Y. Xie and Y. Xiong, *ACS Nano*, 2012, **11**, 9797-9806.
29. R. Narayanan and M. A. El-Sayed, *J. Am. Chem. Soc.*, 2004, **126**, 7194-7195.
30. N. Ortiz and S. E. Skrabalak, *Angew. Chem., Int. Ed.*, 2012, **51**, 11757-11761.
31. J. Watt, N. Young, S. Haigh, A. Kirkland and R. D. Tilley, *Adv. Mater.*, 2009, **21**, 2288-2293.
32. X. Guo and Y. Tan, *Phys. Chem. Chem. Phys.*, 2015, **17**, 31956-31965.
33. N. Ortiz and S. E. Skrabalak, *Cryst. Growth Des.*, 2011, **11**, 3545-3550.
34. A. Mayoral, C. Magen and M. Jose-Yacaman, *Cryst. Growth Des.*, 2011, **11**, 4538-4543.
35. Y. Wang, P. H. C. Camargo, S. E. Skrabalak, H. Gu and Y. Xia, *Langmuir*, 2008, **24**, 12042-12046.
36. P. Lignier, R. Bellabarba, R. P. Tooze, Z. Su, P. Landon, H. Ménard and W. Zhou, *Cryst. Growth Des.*, 2012, **12**, 939-942.
37. N. Tian, Z.-Y. Zhou, S.-G. Sun, L. Cui, B. Ren and Z.-Q. Tian, *Chem. Commun.*, 2006, **2006**, 4090-4092.
38. S.-W. Kim, J. Park, Y. Jang, Y. Chung, S. Hwang, T. Hyeon and Y. W. Kim, *Nano Lett.*, 2003, **3**, 1289-1291.
39. D. Li, C. Wang, D. Tripkovic, S. Sun, N. M. Markovic and V. R. Stamenkovic, *ACS Catalysis*, 2012, **2**, 1358-1362.
40. J. Watt, S. Cheong, M. F. Toney, B. Ingham, J. Cookson, P. T. Bishop and R. D. Tilley, *ACS Nano*, 2010, **4**, 396-402.
41. Z. Fang, Y. Zhang, F. Du and X. Zhong, *Nano Res.*, 2008, **1**, 249-257.
42. A. A. Chernov, *Sov. Phys.-Crystallogr.*, 1972, **16**, 734-753.
43. J. Chen, Y. Xiong, Y. Yin and Y. Xia, *Small*, 2006, **2**, 1340-1343.
44. Z. A. Peng and X. Peng, *J. Am. Chem. Soc.*, 2001, **123**, 1389-1395.
45. L. Manna, L. W. Wang, R. Cingolani and A. P. Alivisatos, *J. Phys. Chem. B*, 2005, **109**, 6183-6192.
46. Y. Liu, C. Wang, Y. Wei, L. Zhu, D. Li, J. S. Jiang, N. M. Markovic, V. R. Stanenkovic and S. Sun, *Nano Lett.*, 2011, **11**, 1614-1617.
47. S. Guo, S. Zhang, D. Su and S. Sun, *J. Am. Chem. Soc.*, 2013, **135**, 13879-13884.
48. J. Watt, S. Cheong and R. D. Tilley, *Nano Today*, 2013, **8**, 198-215.
49. S. Cheong, J. Watt and R. D. Tilley, *Nanoscale*, 2010, **2**, 2045-2053.
50. C. Wang, H. Daimon, T. Onodera and T. Koda, *Angew. Chem., Int. Ed.*, 2008, **120**, 3644-3647.
51. D. Farrell, S. A. Majetich and J. P. Wilcoxon, *J. Phys. Chem. B*, 2003, **107**, 11022-11030.
52. Z. Peng, H. You and H. Yang, *ACS Nano*, 2010, **4**, 1501-1510.
53. X. Zhong, Y. Feng, I. Lieberwirth and W. Knoll, *Chem. Mater.*, 2006, **18**, 2468-2471.
54. F. Dumestre, B. Chaudret, C. Amiens, M.-C. Froman, M.-J. Casanove, P. Renaud and P. Zurcher, *Angew. Chem., Int. Ed.*, 2002, **41**, 4286-4289.
55. G. Collins, M. Schmidt, C. O'Dwyer, J. D. Holmes and G. P. McGlacken, *Angew. Chem., Int. Ed.*, 2014, **53**, 4142-4145.
56. S.-B. Wang, W. Zhu, J. Ke, M. Lin and Y.-W. Zhang, *ACS Catal.*, 2014, **4**, 2298-2306.
57. S. Sreedhala, V. Sudheeshkumar and C. P. Vinod, *Nanoscale*, 2014, **6**, 7496-7502.
58. Y. L. X. Huang, Y, Li, H. Zjou, X. Duan, Y. Huang., *Nano Lett.*, 2012, **12**, 4265 - 4270.
59. C. Li, R. Sato, M. Kanehara, H. Zeng, Y. Bando and T. Teranishi, *Angew Chem., Int. Ed.*, 2009, **48**, 6883-6887.
60. F. Wang, C. Li, L.-D. Sun, H. Wu, T. Ming, J. Wang, J. C. Yu and C.-H. Yan, *J. Am. Chem. Soc.*, 2011, **133**, 1106 - 1111.
61. G. Collins, M. Schmidt, C. O'Dwyer, G. McGlacken and J. D. Holmes, *ACS Catal.*, 2014, **4**, 3105 - 3111.